

# MINERALOGY AND ACID NEUTRALISATION MECHANISMS IN INLAND ACID SULFATE ENVIRONMENTS

**IRSHAD BIBI**  
M.Sc. (Hons) Agri

A THESIS SUBMITTED TO THE FULFILMENT OF THE REQUIREMENTS  
FOR THE DEGREE OF DOCTOR OF PHILOSOPHY

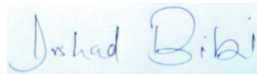
Faculty of Agriculture and Environment  
The University of Sydney, Sydney  
New South Wales  
Australia



## **CERTIFICATE OF ORIGINALITY**

I hereby declare that the text of this thesis is my own work, and that, to the best of my knowledge and belief, it contains no material that has been previously published or written by another person, nor any material that has been accepted as part of the requirements for any other degree or diploma in any university or other institute of higher learning, unless due acknowledgement has been made.

I also declare that the intellectual content of this thesis is original and the result of my own research and to the best of my knowledge and belief, any assistance I received in the experimentation presented, and all sources of information cited have been duly acknowledged.



---

Irshad Bibi

Declared at The University of Sydney

this 22<sup>nd</sup> day of March 2012

**TO  
MY PARENTS  
AND FAMILY**

## ABSTRACT

Soils and sediments containing iron sulfides or the products of sulfide oxidation are known as acid sulfate soils (ASS). These soils possess significant environmental risks due to their potential capacity to produce copious amounts of sulfuric acid ( $\text{H}_2\text{SO}_4$ ) on their exposure to atmosphere. The accumulation of large deposits of sulfidic material has been identified in the past 10 to 12 years in saline-inland wetlands in Australia. Extended periods of natural as well as human-induced drying events in many of these wetlands have resulted in highly saline conditions (e.g. dominated by NaCl and sulfate containing salts) and the exposure (oxidation) of sulfidic material. The oxidation of sulfidic material results in the release of  $\text{H}_2\text{SO}_4$  and the precipitation of a range of secondary iron minerals (e.g. goethite, ferrihydrite, schwertmannite). Under highly acidic conditions ( $\text{pH} < 4$ ) found in sulfuric material of the ASS, dissolution of layer silicates or phyllosilicate minerals is the only realistic process that can provide a long-term acid neutralisation in these soils; particularly in many Australian soils which have small quantities of weatherable primary minerals and carbonates. It is vital to investigate the mineralogical composition and dissolution mechanisms of layer silicates or phyllosilicate minerals existing in these ASS environments to develop effective management strategies for these soils.

The dissolution rate of illite, a common phyllosilicate mineral in Australian soil, was determined using flow-through reactors at  $25 \pm 1^\circ\text{C}$ , in solutions with two different ionic strengths of 0.25 M and 0.01 M (maintained using NaCl), and pH ranging from 1–4.25 ( $\text{H}_2\text{SO}_4$ ). The results from the illite dissolution experiments showed a rapid release of cations at the onset of the experiments and a relatively slower release at the steady state. Close to

stoichiometric dissolution of illite was obtained at pH 1–4 in the higher ionic strength solutions and at pH 1–3 in the lower ionic strength solutions. The experiment at pH 4.25 in the lower ionic strength solution exhibited  $R_{Al} < R_{Si}$ , resulting from a possible adsorption of dissolved Al on the illite surface. Illite dissolution rates showed strong pH dependence, with decreased dissolution rates with increasing pH. The proton reaction orders obtained for dissolution in the higher and lower ionic strength solutions were 0.32 and 0.36, respectively. From the relative cation release data, it was concluded that the dissolution of illite proceeded with the removal of interlayer K followed by the dissolution of octahedral cations, whereas the dissolution of Si was the rate limiting step in the dissolution process.

The dissolution rate of illite, kaolinite and montmorillonite was compared in flow-through reactors at  $25 \pm 1^\circ\text{C}$  and at the two ionic strengths, as described earlier. Kaolinite dissolution rates were close to stoichiometric at pH 1 and 2 in the higher ionic strength solutions and at pH 1–4 in the lower ionic strength solutions.  $R_{Al}$  values greater than  $R_{Si}$  were obtained for kaolinite dissolution experiments at pH 3 and 4 in the higher ionic strength solutions. Kaolinite dissolution rates were strongly dependent on pH at  $\text{pH} \leq 3$ , whereas kaolinite rates showed a little pH dependence at pH 3–4.25, and the point of zero charge (PZC) of the mineral appears to have affected the dissolution rate at these pH values. Kaolinite dissolution rates at pH 1 and 2 ( $\text{H}_2\text{SO}_4$ ) in this study were greater than the previously reported rates in HCl and  $\text{HClO}_4$  solutions, which was ascribed to the complexation of Al by sulfate ions in the solutions. For montmorillonite dissolution,  $R_{Al}$  values greater than  $R_{Si}$  were obtained in the higher ionic strength solutions at pH 1–4, whereas an opposite trend was observed in the lower ionic strength solutions at pH 2–4. A reduced  $R_{Al}$  in the lower ionic strength solutions from montmorillonite dissolution resulted from (apparent) adsorption of dissolved Al on

mineral exchange sites, possibly due to the availability of more interlayer exchange sites for Al re-adsorption and a decreased cation ( $\text{Na}^+$ ) competition for exchange sites in these systems.

The dissolution rate of the clay fraction of soil cores from an inland ASS at Bottle Bend (BB) in south-western New South Wales (NSW, Australia) was determined under similar experimental conditions to pure minerals described earlier. Clay dissolution experiments were also conducted at 35 and 45°C at pH 1 and 4 to determine the effect of temperature on dissolution rates. The clay sample comprised of smectite (40 %), illite (27 %), kaolinite (26 %) and quartz (6 %), with a minor impurity of anatase (1 %). Clay dissolution rates decreased with an increasing pH and a decreasing temperature. A strong reduction in the initial Al release resulted from clay dissolution in the lower ionic strength solutions at pH 2 to 4, whereas a preferential initial Al release was obtained in the higher ionic strength solutions. A slight increase in the  $R_{\text{Si}}$  values was observed at the lower ionic strength across the pH range investigated, whereas a significant decrease in  $R_{\text{Al}}$  was found at pH 4 with a decrease in the ionic strength, at all temperatures. An apparent activation energy value of 18.3 kcal mol<sup>-1</sup> was calculated at pH 1 that decreased to 9.0 kcal mol<sup>-1</sup> at pH 4. The individual mineral dissolution rates estimated from bulk release rate of Al and Si showed fastest dissolution rates for kaolinite followed by illite and smectite. Smectite dissolution rates obtained for soil clay showed close similarity to pure montmorillonite rates obtained under similar conditions. The acid neutralisation capacity (ANC) of the clay sample was calculated from the release rates of cations (Al, Fe, K, Mg). The ANC values of 44.4 and 13.1 kg H<sub>2</sub>SO<sub>4</sub>/tonne of clay sample were estimated from the cation release over a period of 22 and 62 days at pH 1 and 4, respectively. An enhanced release of Al from phyllosilicate dissolution in the highly saline-

acidic systems could possibly be a contributing factor to the ecological disturbance caused by increased Al concentrations in the soil and water systems.

Morphology of the oxidised surface (5 cm) sediments collected from a highly saline inland ASS at the BB site was characterised by X-ray diffraction (XRD), transmission electron microscopy (TEM) and scanning transmission electron microscopy combined with energy dispersive X-ray spectroscopy (STEM-EDS). Halite (NaCl), gypsum ( $\text{CaSO}_4 \cdot 2\text{H}_2\text{O}$ ) and akaganéite ( $\beta\text{-FeOOH}$ ) were identified as the major phases with minor amounts of K-jarosite in some sediment samples. Akaganéite is rarely found in the soil environments and mainly forms as a product of corrosion of iron in chloride-rich environment. The precipitation of akaganéite at the study site resulted from the natural occurrence of the unique solution conditions (*in situ* pH as low as 2 and EC as high as 216 dS/m) at the site. The chemical analysis of the akaganéite found in these sediments revealed an average Fe/Cl mole ratio of 6.7 and a structural formula of  $\text{Fe}_8\text{O}_8(\text{OH})_{6.8}(\text{Cl})_{1.2}$  which is consistent with the composition of pure akaganéite. Saline-acidic conditions with significantly higher chloride over sulfate levels provided the necessary conditions for akaganéite formation at the study site. The precipitation of akaganéite in the ASS environment necessitates detailed investigation to determine the competitive formation and stability of this mineral relative to stable secondary iron minerals commonly precipitated in ASS environments.

\* \* \*

## **ACKNOWLEDGEMENTS**

I am thankful to The University of Sydney for awarding me a (USydIS) PhD scholarship to start my postgraduate studies here at The University of Sydney in Australia. I am highly grateful to my supervisor, Associate Professor Balwant Singh who always travelled above and beyond his responsibility as a supervisor in all aspects of my candidature. He has been deeply involved and dedicated in my research endeavours at all times – from the very start of my candidature until the end of my thesis submission. I thank you for your sincere and substantial efforts to initiate this project, guiding and encouraging me, and most importantly, for maintaining a high level of contact with me throughout the last years of my PhD. I am grateful to you for your support and efforts during the sample collection in the field. I must say that I have learnt it from you to offer high level of passion and devotion to science. I would like to sincerely thank Associate Professor Ewen Silvester (Associate Supervisor) for his substantial contribution, from initial planning of the research project to the interpretation of research data, and the thorough review of my thesis. My sincere thanks goes to Ms Kerry Whitworth who helped me in the field, and carried out the acid sulfate solution analyses and Dr Mark Fraser for his assistance in the field. I am grateful to Dr Jiwchar Ganor (Bengurion University of The Negav, Isreal) for advice and help in the development of experimental set-up and in the analytical methods used in dissolution studies. Dr F. Javier Huertas (Universidad de Granada, Spain) is highly acknowledged for his helpful advice in the experimental set-up development, and a critical review of a draft paper. My heartily thanks to Dr Ian Kaplin (Australian centre for Microscopy and microanalysis, The University of Sydney) who introduced me to the intriguing world of scanning and transmission electron



microscopy techniques and provided me with enormous help in developing the skills necessary for the examination of clay samples.

Thanks to Dr Hank De Bruyn (The University of Sydney) for help with using thermogravimetric analyser; Dr Robert A. Caldwell (The University of Sydney) for his help with freeze drying of clay samples; Ms Pushpinder Matta (Primary Industries, Australia) and Ms Khwunta Khawmee (Kasetsart University, Bangkok) for their help in the sample collection and analytical measurements; Tom Savage (The University of Sydney) for his invaluable assistance in ICP-AES analyses. My sincere thanks go to Dr Rob Fitzpatrick (CSIRO, Adelaide) who provided his valuable suggestions in the planning of this research project. My thanks to Dr Ting-Yu Wang (The University of Sydney) for his assistance in the STEM-EDS analyses of the sediments and the data analyses. I would also like to thank the Associate Editors and referees from *Geochimica et Cosmochimica Acta* for a thorough review of the published papers presented in this thesis. The bulk of this research would not have been possible without generous funding from several sources. I would like to acknowledge the financial support for this project provided by The National Water Commission some through its National Water Standards Program.

I am thankful to Dr Edith Lees for providing constructive comments on review chapter of this thesis. Thanks are extended to the technical staff, Ms Loraine Watson and Ms Iona Georgy for their assistance. Many thanks to the administration staff, Ms Pamela Stern, Ms Prue Winkler, Ms Fortunée Cantrell, Ms. Nancy Cheng and Ms Rocio Pizzaro Marroquin for providing me with overwhelming levels of logistical support throughout the course of my study. I would also like to thank Dr Damien Field (Associate Dean) for his advice and

guidance on different matters during my PhD candidature. I am also thankful to all my friends at Faculty of Agriculture and Environment and colleagues in my research group for their assistance whenever I needed.

I am thankful to Almighty God Who has blessed me with this much of strength, passion and courage to complete my studies. I am thankful to my husband, Nabeel for his tremendous support and encouragement throughout my PhD career and particularly in the last few months of my thesis writing and for proof reading most of my thesis. I would like to thank my son Aaish Khan who has been the source of immense pleasure for me since the moment of his birth. And I would like to dedicate this thesis to my parents who always encouraged me to work hard and fulfil my ambitions, and my deepest love to my brother and sisters, nephews and nieces, and my in-laws.

## PUBLICATIONS

### Refereed scientific journals (Published/submitted)

1. Bibi I, Singh B, Silvester E (2011) Dissolution of illite in saline-acidic solutions at 25°C. *Geochimica et Cosmochimica Acta* 75 (11):3237–3249.
2. Bibi I, Singh B, Silvester E (2011) Akaganéite ( $\beta$ -FeOOH) precipitation in inland acid sulfate soils of south-western New South Wales (NSW), Australia. *Geochimica et Cosmochimica Acta* 75 (21):6429–6438.
3. Bibi I, Singh B, Silvester E (2012) A comparative study of the dissolution kinetics of kaolinite, illite and montmorillonite under acid sulfate conditions. *Clay Minerals* (To be Submitted).

### Refereed scientific journals (In preparation)

4. Bibi I, Singh B, Silvester E (2012) Kinetics of clay dissolution in sulphuric acid solutions: ionic strength and temperature effect. *Geochimica et Cosmochimica Acta* (In preparation).
5. Khawmee K, Suddhiorakaran A, Kheoruenromne I, **Bibi I**, Singh B (2012) Dissolution behaviour of kaolinites from tropical soils. *Geochimica et Cosmochimica Acta* (In preparation).

### Conference paper (refereed)

6. Bibi I, Singh B, Silvester E (2010) Dissolution of phyllosilicates under saline acidic conditions. *Published paper presented in the Proceedings of the 19<sup>th</sup> World Congress of Soil Science on Soil Solutions for a Changing World*, Brisbane, Australia, 1–6 August 2010, pp. 36–39.

### Conference proceedings (abstracts/extended abstracts)

7. Bibi I, Singh B, Silvester E (2010) Dissolution of kaolinite, illite and montmorillonite in acid-saline solutions. *Proceedings of the SEA-CSSJ-CMS Trilateral Meeting on Clays*, Seville, Spain, 6–11 June, 2010 (Poster presentation).
8. Bibi I, Singh B, Silvester E (2010) Experimental study of the effect of saline acidic conditions on illite dissolution. *Proceedings of the SEA-CSSJ-CMS Trilateral Meeting on Clays*, Seville, Spain, 6–11 June, 2010 (Oral presentation).
9. Bibi I, Singh B, Silvester E (2010) Measuring dissolution rates of illite un saline-acidic solutions using flow-through reactors. *Proceedings of the 21<sup>st</sup> Australian Clay Minerals Conference*, Brisbane, Australia, 7–8 August 2010 (Poster presentation).

10. Bibi I, Singh B, Silvester E (2010) Akaganéite ( $\beta$ -FeOOH) precipitation in inland acid sulfate soils of south-western New South Wales. *Proceedings of the 21<sup>st</sup> Australian Clay Minerals Conference*, Brisbane, Australia, 7–8 August, 2010 (Oral presentation).
11. Bibi I, Singh B, Silvester E (2011) Akaganéite formation in inland wetlands with sulfidic sediments in Australia. *Proceedings of the 48<sup>th</sup> Annual Meeting of The Clay Minerals Society*, Stateline, Nevada, USA, 24–29 September, 2011 (Oral presentation).
12. Bibi I, Singh B, Silvester E (2011) Dissolution of common phyllosilicates in acid sulfate systems. *Proceedings of the ASA, CSSA, SSSA International Annual Meetings. Fundamental for Life: Soil, Crop and Environmental Sciences*, San Antonio, Texas, USA, 16–19 October, 2011 (Poster presentation).
13. Bibi I, Singh B, Silvester E (2012) Dissolution of clay sediments in acid-sulfate systems. *Proceedings of the Australian Regolith and Clays Conference*, Mildura, Australia, 7–10 February, 2012 (Oral presentation).
14. Bibi I, Singh B, Silvester E (2012) Inland wetlands with sulfidic sediments provide ideal conditions for Akaganéite. *Proceedings of the Australian Regolith and Clays Conference*, Mildura, Australia, 7–10 February, 2012 (Oral presentation).

#### **Poster presentation**

15. Bibi I, Singh B, Silvester E (2010) Clay minerals dissolution in acid sulfate environment. *The 'Centenary Research Symposium' of The Faculty of Agriculture, Food and Natural Resources, The University of Sydney*, 4 June 2010.

## **TABLE OF CONTENTS**

<b>ABSTRACT</b>	<b>iii</b>
<b>ACKNOWLEDGEMENTS</b>	<b>vii</b>
<b>PUBLICATIONS</b>	<b>x</b>
<b>TABLE OF CONTENTS</b>	<b>xii</b>
<b>LIST OF FIGURES</b>	<b>xix</b>
<b>LIST OF TABLES</b>	<b>xxiii</b>

## CHAPTER 1

---

### **General Introduction** **1**

<b>1.1</b>	<b>Introduction</b>	<b>1</b>
<b>1.2</b>	<b>Aims</b>	<b>5</b>
<b>1.3</b>	<b>Objectives</b>	<b>5</b>
<b>1.4</b>	<b>References</b>	<b>7</b>

## CHAPTER 2

<b>Review of Literature</b>	<b>12</b>
<b>2.1 Acid sulfate soils</b>	<b>12</b>
2.1.1 Iron sulfide formation and oxidation	13
2.1.2 Factors determining types of secondary iron minerals in ASS	18
2.1.3 Secondary iron minerals associated with pyrite oxidation	20
2.1.4 Transformation of metastable iron minerals to goethite	22
<b>2.2 Extent and Distribution of ASS: worldwide and in Australia</b>	<b>29</b>
2.2.1 Development of inland ASS in Australia	32
<b>2.3 Acid neutralisation processes in ASS</b>	<b>34</b>
2.3.1 Carbonate and silicate dissolution	34
2.3.2 Precipitation of secondary mineral phases	36
2.3.3 Dissolution of phyllosilicate minerals in saline acidic solutions	37
2.3.3.1 Effect of temperature	43
2.3.3.2 Effect of saturation	46
2.3.3.3 Effect of ionic strength	49
<b>2.4 References</b>	<b>51</b>

---

**CHAPTER 3**

<b>Dissolution of illite in saline–acidic solutions at 25°C</b>	<b>64</b>
<b>Abstract</b>	<b>64</b>
<b>3.1 Introduction</b>	<b>65</b>
<b>3.2 Materials and Methods</b>	<b>67</b>
3.2.1 Pre–treatment and characterization	67
3.2.2 Flow-through dissolution experiments	69
3.2.3 Solution phase analyses	71
3.2.4 Solid phase analyses	72
<b>3.3 Kinetics calculations</b>	<b>72</b>
<b>3.4 Results</b>	<b>74</b>
<b>3.5 Discussion</b>	<b>89</b>
3.5.1 Fast Initial Dissolution Rates	89
3.5.2 Stoichiometry of dissolution reaction	90
3.5.3 Release of K, Fe and Mg from illite	93
3.5.4 Saturation state of the steady state solutions	96
3.5.5 Dissolution rates of illite at the steady state and a comparison with the previous studies	96
<b>3.6 Conclusions</b>	<b>99</b>
<b>3.7 References</b>	<b>100</b>



---

**CHAPTER 4****Dissolution kinetics of kaolinite, illite and montmorillonite under acid-sulfate conditions: a comparative study** **105**

---

<b>Abstract</b>	<b>105</b>
<b>4.1 Introduction</b>	<b>106</b>
<b>4.2 Materials and Methods</b>	<b>109</b>
4.2.1 Clay pre-treatment and characterisation	109
4.2.2 Flow-through reactor dissolution experiments	111
4.2.3 Solution phase analysis	111
<b>4.3 Calculations</b>	<b>112</b>
4.3.1 Dissolution rate calculations	112
<b>4.4 Results</b>	<b>113</b>
4.4.1 Initial release rates of elements	113
4.4.2 Relative release rates of elements at the steady state	120
4.4.3 Dissolution rates of minerals	121
4.4.4 Saturation state of the steady state solutions	123
<b>4.5 Discussion</b>	<b>125</b>
4.5.1 Initial release rates	125
4.5.2 Steady state dissolution	126
4.5.3 pH dependence	128
4.5.4 Mineral dissolution rates	130
<b>4.6 Conclusions</b>	<b>133</b>
<b>4.7 References</b>	<b>135</b>

---

**CHAPTER 5****Effect of pH, ionic strength and temperature on clay dissolution in saline-acid sulfate solutions** **140**

---

<b>Abstract</b>	<b>140</b>
<b>5.1 Introduction</b>	<b>141</b>
<b>5.2 Materials and Methods</b>	<b>144</b>
5.2.1 Clay sample	144
5.2.2 Sample pre-treatment and characterisation	144
5.2.3 Chemical composition determination	145
5.2.4 X-ray diffraction analysis	145
5.2.5 Transmission electron microscopic analysis	147
5.2.6 Flow-through reactor dissolution experiments	147
5.2.7 Output solution analyses	148
5.2.8 Geochemical speciation modelling	148
5.2.9 Clay dissolution rates	149
<b>5.3 Results</b>	<b>149</b>
<b>5.4 Discussion</b>	<b>162</b>
5.4.1 Initial release of Si, Al, K, Fe and Mg	162
5.4.2 Stoichiometry of clay dissolution at steady state	166
5.4.3 Effect of pH on clay dissolution rate	168
5.4.4 Effect of temperature on clay dissolution rate	169
5.4.5 Dissolution rates of individual minerals	171
5.4.6 Acid neutralisation capacity of clay	174
5.4.7 Maximum acid neutralisation capacity of clay ( $ANC_{max}$ )	176
<b>5.5 Conclusions</b>	<b>177</b>
<b>5.6 References</b>	<b>179</b>

---

**CHAPTER 6**

**Akaganéite precipitation in inland acid sulfate soils** **186**

---

<b>Abstract</b>	<b>186</b>
<b>6.1 Introduction</b>	<b>187</b>
<b>6.2 Materials and Methods</b>	<b>189</b>
6.2.1 Study site	189
6.2.2 Soil and water sample collection and analyses	190
6.2.3 Random powder XRD and Rietveld analyses	191
6.2.4 TEM, STEM and SEM analyses	192
6.2.5 TGA and FTIR analyses	192
<b>6.3 Results</b>	<b>193</b>
<b>6.4 Discussion</b>	<b>203</b>
6.4.1 Akaganéite occurrence, structure and conditions of formation	203
6.4.2 Formation of akaganéite at Bottle Bend Lagoon	206
6.4.3 On the absence of schwertmannite	208
<b>6.5 Conclusions</b>	<b>209</b>
<b>6.6 References</b>	<b>210</b>

**CHAPTER 7**

**Summary and future research** **216**

---

**APPENDICES** **222**

---

---

## LIST OF FIGURES

### CHAPTER 2

---

- Fig. 2.1** A schematic diagram showing a biogeochemical model for the formation/precipitation of various (secondary) iron minerals occurring in acid mine drainage and acid sulfate soils (modified from Bigham et al., 1992). **19**
- Fig. 2.2** A schematic soil landscape cross section representing the development of saline-acidic land with sulfuric materials, removed vegetation, reduction of wetland biodiversity, poor water quality, and ground subsidence, in an estuary in South Australia (Australia) (modified from Fitzpatrick and Shand 2008) **30**
- Fig. 2.3** The graph showing the acid buffering pH region for cation exchange and soil minerals (carbonates, phyllosilicates). **39**

### CHAPTER 3

---

- Fig. 3.1** Schematic representation diagram of (a) flow-through reactor, and (b) experimental set-up used for the flow through dissolution experiments. **70**
- Fig. 3.2** Transmission electron microscope images of illite (a) after pre-treatment, and (b) after dissolution (steady state conditions established) at pH 2.06 and ionic strength 0.25 (M). **76**
- Fig. 3.3** Relative release rates of Al and K over Si as a function of time at pH 1–4 and at 0.25 (M) ionic strength. Figures 3.3 (a), (c), (e) and (g) show Al/Si ratios for pH 1–4 respectively; Figures 3.3(b), (d), (f) & (h) show K/Si ratios for pH 1–4, respectively. **80**
- Fig. 3.4** Relative release rates of Al and K over Si as a function of time at pH 1–4.25 and at 0.01 (M) ionic strength. Figures 3.4 (a), (c), (e) and (g) show Al/Si ratios for pH 1–4.25, respectively. Figures 3.4 (b), (d), (f) and (h) show K/Si ratios for pH 1–4.25, respectively. **81**
- Fig. 3.5** Steady state log concentrations ( $\mu\text{mol/L.g}$ ) of K as a function of pH for high ( $I = 0.25$  M) and low ( $I = 0.01$  M) ionic strength systems. **83**
- Fig. 3.6** Aqueous speciation of: (a) Al and (b) Fe in the steady state output solutions at high ( $I = 0.25$  M) ionic strength. Al concentrations used for aqueous speciation are 4.16, 5.56, 3.66 and 0.62  $\mu\text{M}$  at pH 1, 2, 3 and 4, respectively. Fe concentrations used for speciation calculations are 1.70, 2.70, 0.60 and 0.17  $\mu\text{M}$  at pH 1, 2, 3 and 4, respectively. **84**
- Fig. 3.7** Aqueous speciation of: (a) Al and (b) Fe in the steady state output solutions at low ( $I = 0.01$  M) ionic strength. Al concentrations used for aqueous speciation are 9.92, 4.21, 2.53 and 0.42  $\mu\text{M}$  at pH 1, 2, 3 and 4.25, respectively. Fe concentrations used for speciation calculations are 2.69, 2.90, 1.42 and 0.74  $\mu\text{M}$  at pH 1, 2, 3 and 4.25, respectively. **85**

- Fig. 3.8** Illite dissolution rates (from Si-release data) obtained in this study at pH 1–4,  $I = 0.25\text{M}$  ( $y = -0.318x - 12.485$ ,  $R^2 = 0.978$ ) and  $0.01\text{ M}$  ( $y = -0.363x - 12.38$ ,  $R^2 = 0.990$ ) and the dissolution rates obtained using batch reactors at pH 1–4,  $I = 0.1\text{ M}$  (Kohler et al. 2003;  $y = -0.6387x - 11.604$ ,  $R^2 = 0.9753$ ). The data points for the dissolution rates of kaolinite (Cama et al. 2002;  $y = -0.325x - 12.644$ ,  $R^2 = 0.9518$ ) and montmorillonite (Rozalen et al. 2008;  $y = -0.3184x - 12.497$ ,  $R^2 = 0.972$ ) obtained using flow-through reactors are also plotted for comparison. Log  $R_{Si}$  at  $I = 0.25\text{ M}$  (●) and  $0.01\text{ M}$  (○), in this study; log  $R_{Si}$ , (×) kaolinite (Cama et al., 2002); (□) illite (Kohler et al., 2003); (Δ) montmorillonite (Rozalen et al., 2008). **98**

## CHAPTER 4

- Fig. 4.1** Solution pH and the concentrations of Al and Si (a,c,e,g) and Al/Si ratio (b,d,f,h) in the output solution as a function of time for kaolinite dissolution at pH 1–4 and at  $I = 0.25\text{ M}$ . **115**
- Fig. 4.2** Solution pH and the concentrations of Al and Si (a,c,e,g) and Al/Si ratio (b,d,f,h) in the output solution as a function of time for kaolinite dissolution experiments at pH 1–4.25 and at  $I = 0.01\text{ M}$ . **116**
- Fig. 4.3** Solution pH and the concentrations of Al and Si (a,c,e,g) and Al/Si ratio (b,d,f,h) in the output solution as a function of time for montmorillonite dissolution experiments at pH 1–4 and at  $I = 0.25\text{ M}$ . **118**
- Fig. 4.4** Solution pH and the concentrations of Al and Si (a,c,e,g) and Al/Si ratio (b,d,f,h) in the output solution as a function of time for montmorillonite dissolution experiments at pH 1–4.25 and at  $I = 0.01\text{ M}$ . **119**
- Fig. 4.5** (a) The plot of log  $R_{Si}$  versus pH for kaolinite, illite and montmorillonite at the higher ionic strength (0.25). The regression equations for kaolinite, illite and montmorillonite are: log  $R_{Si} = -0.72\text{pH} - 11.55$ ; log  $R_{Si} = -0.32\text{pH} - 12.47$ ; and log  $R_{Si} = -0.22\text{pH} - 12.55$ , respectively. (b) The plot of log  $R_{Si}$  versus pH for kaolinite, illite and montmorillonite at the lower ionic strength (0.01); the regression equations for kaolinite, illite and montmorillonite are: log  $R_{Si} = -0.78\text{ pH} - 11.43$ ; log  $R_{Si} = -0.36\text{ pH} - 12.38$ ; and log  $R_{Si} = -0.26\text{ pH} - 12.35$ , respectively. Kaolinite dissolution data at pH 4 at both ionic strengths was not included in the regression analysis. **129**
- Fig. 4.6** A comparison of kaolinite (KGa-2) dissolution rates log  $R_{Si}$  and log  $R_{Al}$  between pH 1 and 4, obtained in this study ( $I = 0.25$ ) with published data (Cama et al., 2002; Huertas et al., 1999). The data from Cama et al. (2002) is for flow-through reactor experiments using Georgia kaolinite (KGa-2) with pH adjustment using  $\text{HClO}_4$ , whereas the data from Huertas et al. (1999) is from batch dissolution experiments using Georgia kaolinite (KGa-1) in a background electrolyte of  $1\text{M NaCl}$ , with pH adjustment using  $\text{HCl}$ . **131**
- Fig. 4.7** Comparison of dissolution rate (log  $R_{Al}$ ) values for montmorillonite at pH 1–4 at the higher ( $I = 0.25$ ) and lower ( $I = 0.01$ ) ionic strengths. **133**

---

## CHAPTER 5

---

- Fig. 5.1** X-ray diffraction patterns of the oriented specimens of Bottle Bend clay sample (< 2  $\mu\text{m}$ ). Mg air-dried (Mg-AD); Mg ethylene glycolated (Mg-EG); K heated at 550°C (K 550° C); Li heated at 300°C (Li 300°C); Li heated at 300°C and glycerol solvated (Li-300-Gly). **150**
- Fig. 5.2** Transmission electron microscopic image of a pre-treated Bottle Bend clay sample showing three different mineral (particle) types. Smectite particles – irregular to a globular shape, thin layered structure; illite particles – platy shape; kaolinite particles – hexagonal shape. **151**
- Fig. 5.3** Change in Al/Si ratio with time in the experiments conducted at the two ionic strengths (0.25 and 0.01 M) and pH 1–4. (a,c,e,g) 25°C; (b,d) 35°C; (f,h) 45°C. Al/Si ratio in experiments conducted at pH 4 at  $I = 0.01$  M at all temperatures are not shown because of a very low Al release (< 1  $\mu\text{M}$ ) throughout the experimental duration. **155**
- Fig. 5.4** Variation in K/Si ratio with time in the experiments conducted at the two ionic strengths (0.25 and 0.01 M) and pH 1–4. (a,c,e,g) 25°C; (b,d) 35°C; (f,h) 45°C. **156**
- Fig. 5.5** Change in Fe/Si ratio with time in the experiments conducted at the two ionic strengths (0.25 and 0.01 M) and pH 1–4. (a,c,e,g) 25°C; (b,d) 35°C; (f,h) 45°C. **158**
- Fig. 5.6** Change in Mg/Si ratio with time in the experiments conducted at the two ionic strengths (0.25 and 0.01 M) and pH 1–4. (a,c,e,g) 25°C; (b,d) 35°C; (f,h) 45°C. **159**
- Fig. 5.7** Arrhenius plot illustrating the variation in steady state clay dissolution rate,  $\log R_{Si}$  ( $\text{mol m}^{-2}\text{s}^{-1}$ ) against 1000 times reciprocal temperature,  $T$  ( $\text{K}^{-1}$ ) for the experiments performed at pH 1 and 4. Simple linear regression equations for the plotted data ( $\log$  rate vs.  $1000/T$  ( $\text{K}^{-1}$ )) is also presented:  $\log R_{Si} = -3.996x + 1.472$  ( $R^2 = 1$ ), and  $\log R_{Si} = -1.959x - 6.656$  ( $R^2 = 0.99$ ) at pH 1 and 4, respectively. **160**
- Fig. 5.8** A plot of  $\log R_{Si}$  values estimated for individual minerals (kaolinite, illite and smectite) based on the content of each mineral in the bulk clay sample as a function of pH (1–4) and at  $I = 0.25$  M in this study; and a comparison of these rates with  $\log R_{Si}$  values from previous studies on pure mineral samples of kaolinite, illite and smectite. **174**

---

## CHAPTER 6

---

- Fig. 6.1** X-ray diffraction patterns of five acid sulfate sediments: (a) before washing treatment showing major peaks for gypsum (the dominant mineral in all samples), d-spacing values for gypsum peaks mentioned in angstrom ( $\text{\AA}$ ). For quartz (Q), K-jarosite (J), halite (H) and akaganéite (A), peaks are indicated by alphabets. (b) X-ray diffraction patterns of five samples after washing with E-pure® water, 0.01 M HCl and 0.01 M EDTA solutions. All washed samples contain akaganéite as the dominant phase (akaganéite peaks indicated by d-spacing values in angstrom), with lesser amounts of gypsum (G), K-jarosite (J), mica (M) and quartz (Q). Bassanite (B) was formed from gypsum in S2 sample after the washing treatment. All diffraction peaks on Figures 1a and 1b are given in  $\text{\AA}$ . **196**
- Fig. 6.2** Rietveld refinement plot of a washed sample (#1). **197**
- Fig. 6.3** Transmission electron microscopic images of sample #1 (a) before and (b) after the removal of salts. The images show a spindle-shaped morphology for the akaganéite particles; and the treatment applied to dissolve halite and gypsum from the sediments did not affect the morphology of akaganéite particles. **200**
- Fig. 6.4** Scanning electron micrographs of an original acid sulfate surface sample (#1) showing aggregates of small-sized akaganéite particles and large sized (a) gypsum and (b) halite crystals. **202**

- Fig. 6.5** (a & c) Bright field scanning transmission electron microscope images of akaganéite particles (#1) at two different locations. The arrows in the images show the section of the particle selected for a line scan EDS analysis; (b & d) show the quantified composition (atomic %) of Fe, O and Cl in akaganéite plotted against the number of points selected, corresponding to the arrows shown in (a) & (c). **203**
- Fig. 6.6** E<sub>H</sub>-pH diagram for Fe-S-Cl-H<sub>2</sub>O system at 25°C. (a) shows the stability field of akaganéite, excluding: all Fe<sup>III</sup> (oxyhydr)oxide phases except Fe(OH)<sub>3</sub>, all jarosite minerals and schwertmannite. (b) shows the stability fields of akaganeite and K-jarosite (excluding the same set of minerals described for (a), except K-jarosite). Stability diagrams calculated using Geochemical Workbench. **204**
- Fig. 6.7** FTIR spectra of synthetic akaganéite and sample #1 after washing treatments to remove soluble salts and gypsum. **205**
- Fig. 6.8** TGA curves of (a) synthetic akaganéite and (b) sample #1 after washing treatments to remove soluble salts and gypsum. **206**

---

## LIST OF TABLES

### CHAPTER 2

---

<b>Table 2.1</b>	Summary of the occurrence and distribution of secondary Fe oxides, sulfides, carbonates and salts in soil environment (modified from Fitzpatrick et al., 2008).	<b>17</b>
<b>Table 2.2</b>	Selected log normalised dissolution rates (based on Si and/or Al release) and reaction orders (n) of kaolinite, illite and smectite at 25°C.	<b>38</b>
<b>Table 2.3</b>	Activation energies for dissolution kinetics of kaolinite, illite and montmorillonite under acidic conditions.	<b>44</b>

### CHAPTER 3

---

<b>Table 3.1</b>	The atomic ratios for Silver Hill Illite calculated from its chemical composition determined by XRF analysis.	<b>69</b>
<b>Table 3.2</b>	Summary of the experimental conditions, steady state concentrations ( $\mu\text{mol/L.g}$ ) of Al, Si and K, element release ratios (Al/Si, K/Si, Fe/Si, Mg/Si) and dissolution rates calculated for illite dissolution at 0.25 and 0.01 (M) ionic strength (I) and at 25°C.	<b>77</b>
<b>Table 3.3</b>	Saturation state (in terms of Gibbs free energy, $\Delta G$ , kcal/mol), of the steady state solutions at ionic strength (I) = 0.25 and 0.01 and at pH range 1.0-4.25 with respect to selected minerals.	<b>88</b>

### CHAPTER 4

---

<b>Table 4.1</b>	The atomic ratios of cationic elements with Si for Georgia Kaolinite (KGa-2), Wyoming montmorillonite (SWy-2) and Silver Hill Illite (IMt-2) Na-saturated samples calculated from their chemical compositions determined by X-ray fluorescence (XRF) analyses.	<b>120</b>
<b>Table 4.2</b>	Atomic ratios (Al/Si, Fe/Si and Mg/Si) in the steady state solutions for the two ionic strength solutions at pH 1–4.25 at 25°C.	<b>121</b>
<b>Table 4.3</b>	Experimental conditions, steady state concentrations of cations ( $\mu\text{mol/L.g}$ ) in the output solution and mineral dissolution rates ( $\text{mol m}^{-2} \text{s}^{-1}$ ) at 25°C.	<b>122</b>
<b>Table 4.4</b>	Saturation state of the steady state solutions for kaolinite dissolution experiments with respect to selected minerals.	<b>124</b>
<b>Table 4.5</b>	Saturation state of the steady state solutions for montmorillonite dissolution experiments with respect to selected minerals.	<b>124</b>



---

## CHAPTER 5

---

<b>Table 5.1</b>	Bulk chemical composition (XRF) of Na-saturated Bottle Bend (BB) clay fraction.	<b>146</b>
<b>Table 5.2</b>	Atomic ratios of major cations with Si for the BB clay calculated from X-ray fluorescence (XRF) analysis.	<b>146</b>
<b>Table 5.3</b>	Summary of experimental conditions, steady state concentrations ( $\mu\text{mol/L}$ ) of Si, Al, K, Fe and Mg and elemental ratios calculated from the dissolution experiments at pH 1–4, at $I = 0.25$ M and 0.01 M at 25–45°C.	<b>153</b>
<b>Table 5.4</b>	Saturation state of the steady state solutions at $I = 0.25$ M and 0.01 M and at pH 1–4 at a solution temperature range of 25–45°C.	<b>161</b>
<b>Table 5.5</b>	Estimated dissolution rates ( $\text{mol m}^{-2} \text{s}^{-1}$ ) of kaolinite, illite and smectite at pH 1–4 at 25°C and at pH 1 and 4 at 35°C and 45°C.	<b>173</b>
<b>Table 5.6</b>	The acid neutralisation capacity (ANC) values in $\text{kg H}_2\text{SO}_4/\text{t}$ of clay sample calculated from the cation release at pH 1–4 and $I = 0.25$ M.	<b>176</b>

---

## CHAPTER 6

---

<b>Table 6.1</b>	The composition of surface and ground water samples at Bottle Bend lagoon in New South Wales, Australia (February 2009).	<b>195</b>
<b>Table 6.2</b>	Results of the Rietveld quantification of washed sediment samples (1–5). The contents are presented as wt.%; $R_p$ , $R_{pb}$ , $R$ , $R_{wp}$ and $R_{exp}$ are in %.	<b>199</b>
<b>Table 6.3</b>	Structural formula of akaganéite calculated from the STEM-EDS analyses of particles.	<b>201</b>